JOURNAL OF SPACECRAFT AND ROCKETS
Vol. 35, No. 6, November–December 1998

Launch Vehicle Trajectories with a Dynamic Pressure Constraint

Sang-Young Park*
Texas A&M University, College Station, Texas 77843

The problem of three-dimensional launch trajectories for the advanced launch system to minimize fuel or equivalently maximize payload is considered. A dynamic pressure inequality constraint is involved due to its significance on the resulting trajectories and structure of the launch vehicle. Highly accurate solutions and exact switching structures of the optimal trajectories are presented by using a multiple shooting method. The multiple shooting structure is modified to satisfy the internal boundary conditions and discontinuities in variables at entry and exit points of the boundary arc. A methodology is also developed to visualize the optimal controls in a geometric sense using hodograph analysis.

Nomenclature

A_b = cross-sectional area
A_e = exit area of a engine
a = speed of sound
C_D = drag coefficient
C_L = lift coefficient
C_m = pitching moment coefficient
$C_{m\text{cg}}$ = pitching moment coefficient about the center of gravity
c = number of engines operating
D = drag
e = eccentricity of orbit
$\boldsymbol{f}$ = dynamic equations
G = function of states, controls, and time
g = Earth's gravitational force
g_s = Earth's gravitational force at sea level
H = Hamiltonian function
h = altitude above mean sea level
h_a = apogee altitude
h_f = altitude at t_f
h_p = perigee altitude
h_1 = density scale height
h_2 = pressure scale height
I_{sp} = specific impulse
J = performance index
L = lift
l = total core vehicle length
l_T = distance from the center of mass to the exit plane of engine
M = Mach number
M_{aero} = aerodynamic pitching moment
M_T = pitching moment due to thrust
m = mass
m_{ref} = reference mass, sum of the masses of the payload, payload margin, and payload fairing
p = atmospheric pressure
q = dynamic pressure
r = distance from the center of the Earth to the vehicle center of gravity, $r_s + h$
r_a = radius at apogee from the center of the Earth
r_p = radius at perigee from the center of the Earth
r_s = radius of the Earth at sea level
S = state inequality constraint
S^p = pth time derivative of S
T = thrust
T_{vac} = thrust of one engine in a vacuum
t = time
t_{en} = entry point to state inequality
t_{ex} = exit point from state inequality
t_f = free final time
t_s = staging time
t_0 = initial time
$\boldsymbol{u}$ = control variables
$\boldsymbol{u}^*$ = extremal controls
V = velocity
V_{if} = inertial velocity at t_f
$\boldsymbol{x}$ = state variables
$\boldsymbol{x}_0$ = initial state variables
$\boldsymbol{x}^*$ = extremal states
α = angle of attack
α_b = angle of attack as boundary control over boundary arc
β = ratio of specific heats of air
γ = flight-path angle
δ = gimbal angle of the thrust vector
ε = constant Lagrange multiplier
η = constant multiplier of S^p
$\boldsymbol{\Theta}$ = prescribed terminal constraints
Λ = Lagrange multipliers
Λ_x = Lagrange multiplier of x state
Λ^* = extremal costates
λ = longitude
μ = velocity roll angle, positive roll angle results in a negative heading angle toward the south
$\boldsymbol{\nu}$ = constant multiplier vector of the dimension of $\boldsymbol{\Theta}$
ρ = atmospheric density
ρ_s = atmospheric density at sea level
τ = latitude
ϕ = function of final states and time
ψ = heading angle
Ω = set of admissible control values
ω = angular velocity of the Earth

Subscripts

f = at t_f
f_s = specified value at t_f
i = inertial coordinate

Superscripts

$\cdot$ = time derivative
$-$ = just before t_{en}, t_{ex}, or t_s
$+$ = just after t_{en}, t_{ex}, or t_s

Presented as Paper 94-3770 at the AIAA Guidance, Navigation, and Control Conference, Scottsdale, AZ, Aug. 1-3, 1994; received Sept. 8, 1997; revision received Aug. 15, 1998; accepted for publication Aug. 25, 1998.

*Graduate Student, Department of Aerospace Engineering; currently National Research Council Postdoctoral Associate, Department of Aeronautics and Astronautics, U.S. Naval Postgraduate School, Monterey, CA 93943. Member AIAA.

Introduction

MANY problems in the design of modern control and guidance systems require optimization of the trajectory that minimizes

(or maximizes) some performance criterion. Using the theory of the calculus of variations, the formulation of these problems yields a multipoint boundary-value problem (MPBVP). The resulting optimal trajectory also satisfies the physical constraints and the given differential equations. The open-loop optimal trajectory is used as a reference trajectory for perturbation guidance. A variety of techniques is currently available for the solution of trajectory optimization problems. They include shooting methods, gradient methods, and nonlinear programming methods. The family of shooting methods are used when a highly accurate solution is required.

All space missions in the United States are operated by the current expendable launch vehicles and Space Shuttle. However, the cost of this access to space is too high to achieve good reliability and operability of these systems. One of the next generation heavy-lift launch systems considered by NASA and the Department of Defense was the advanced launch system (ALS). The ALS has been used in many studies to demonstrate optimal and suboptimal control and guidance strategies.[1–8] Shaver and Hull[1] present a suboptimal control strategy using parameterization of the control variables. Seywald and Cliff[2] present a feedback control method for two-dimensional flights using neighboring extremals. Hodges et al.[3] and Bless et al.[4] present a finite element method for trajectory optimization in two-dimensional flights. Shelton[5] studied the optimal trajectories for the second stage using a direct shooting method. The complete solution was not obtained in this work due to the sensitivity of the problem. Burkhart[6] calculated the optimal controls for the unconstrained case using the single shooting method. Wirthman et al.[7] present the implementation of the ALS trajectory optimization in two-dimensional flights on a parallel computer. Recently, Burkhart and Hull[8] studied the optimal controls for unconstrained case and compared the results with those of suboptimal control.

In this paper, we present three-dimensional optimal solutions for the constrained ascent trajectories of the ALS using the method of multiple shooting with two slightly different aerodynamic models to obtain highly accurate solutions and an exact switching structure. Two aerodynamic models of the ALS are presented,[1,2] and more can be generated by varying the order of the interpolation technique used to fit the data. Optimal trajectories are generated subject to a dynamic pressure inequality constraint. The algorithm for optimal control problems with state inequality constraints is also referred. The optimality of this transition is analyzed using hodograph analysis. The hodograph exhibits nonconvexity during certain points of time. It is also verified that the optimal state rates during these intervals lie on the convex domains of their respective hodographs.

Optimization Algorithm

Optimal control theory is concerned with finding the control history to optimize a measure of the performance index of the following general form:

$$J(\boldsymbol{u}) = \phi(\boldsymbol{x}(t_f), t_f) + \int_{t_0}^{t_f} G(\boldsymbol{x}, \boldsymbol{u}, t)\,\mathrm{d}t \tag{1}$$

subject to the dynamic equations, boundary conditions, and terminal constraints

$$\dot{\boldsymbol{x}} = \boldsymbol{f}(\boldsymbol{x}, \boldsymbol{u}, t), \qquad \boldsymbol{x}(t_0) \equiv \boldsymbol{x}_0, \qquad t_0 \text{ given} \tag{2}$$

$$\boldsymbol{\Theta}[\boldsymbol{x}(t_f), t_f] = \boldsymbol{0} \tag{3}$$

Here $\boldsymbol{x}(t) \in \boldsymbol{R}^n$, $\boldsymbol{u}(t) \in \boldsymbol{R}^l$, and $\boldsymbol{\Theta} \in \boldsymbol{R}^k$. Assume that the functions G, ϕ, and $\boldsymbol{f}$, respectively, are continuously differentiable with respect to all their arguments. The Hamiltonian function is defined with $\boldsymbol{\Lambda}(t) \in \boldsymbol{R}^n$ as

$$H \equiv G + \boldsymbol{\Lambda}^T \boldsymbol{f} \tag{4}$$

The minimum principle requires that the optimal controls minimize H (Ref. 9)

$$\boldsymbol{u}^*(t) = \min_{u \in \Omega} \arg H(\boldsymbol{x}^*, \boldsymbol{\Lambda}^*, \boldsymbol{u}, t) \tag{5}$$

For the ALS problem, we use the open set of admissible control values. The states, costates, and the Hamiltonian satisfy the following conditions:

$$\dot{\boldsymbol{x}}^T = H_{\boldsymbol{\Lambda}} \tag{6a}$$

$$\dot{\boldsymbol{\Lambda}}^T = -H_{\boldsymbol{x}} \tag{6b}$$

$$\boldsymbol{\Lambda}^T(t_f) = (\phi_{\boldsymbol{x}} + \boldsymbol{\nu}^T \boldsymbol{\Theta}_{\boldsymbol{x}})^{t=t_f} \tag{6c}$$

$$H(t_f) = -(\phi_t + \boldsymbol{\nu}^T \boldsymbol{\Theta}_t)^{t=t_f} \tag{6d}$$

$$\boldsymbol{0} = H_{\boldsymbol{u}} \tag{6e}$$

Equation (6e) can be solved for the control, so that the control is removed from Eqs. (6a) and (6b).

State variable inequality constraints are augmented to the cost function and additional necessary conditions are obtained as a result.[10,11] These necessary conditions, depending on the type of inequality constraint, might require jumps in the costates or the Hamiltonian. Thus, a general optimal control problem requires the solution of a MPBVP. The state inequality constraint is represented as

$$S(\boldsymbol{x}(t)) \equiv q(\boldsymbol{x}) - q_{\max} \le 0, \qquad 0 \le t \le t_f \tag{7}$$

Here $S: \boldsymbol{R}^n \to R$. For the ALS problem, the state inequality constraint is a first-order dynamic-pressure constraint. An optimal trajectory is composed of two types of arcs: interior arcs [$S(\boldsymbol{x}) < 0$] and boundary arcs [$S(\boldsymbol{x}) = 0$]. Excepting junction conditions, an interior arc satisfies the same necessary conditions as the unconstrained problem.[12] Along a boundary arc, the inequality constraint becomes an equality constraint. For numerical convenience,[13] we use the necessary conditions in Ref. 10. The modified Hamiltonian with a pth-order state variable inequality constraint (p times the constraint has to be differentiated with respect to the independent variable to obtain explicit dependence on at least one control variable) is defined as

$$H = G + \boldsymbol{\Lambda}^T \boldsymbol{f} + \eta S^p \tag{8}$$

where

$$\eta \begin{cases} = 0, & \text{if} \quad S < 0 \quad (9a) \\ \ge 0, & \text{if} \quad S = 0 \quad (9b) \end{cases}$$

The necessary conditions on the boundary arcs are

$$H_{\boldsymbol{u}} = G_{\boldsymbol{u}} + \boldsymbol{\Lambda}^T \boldsymbol{f}_{\boldsymbol{u}} + \eta S^p_{\boldsymbol{u}} = 0 \tag{10}$$

$$\dot{\boldsymbol{\Lambda}}^T = -G_{\boldsymbol{x}} - \boldsymbol{\Lambda}^T \boldsymbol{f}_{\boldsymbol{x}} - \eta S^p_{\boldsymbol{x}} \tag{11}$$

The beginning and the end of the constrained arcs are denoted by the times t_{en} and t_{ex}, respectively. At t_{en}, $S^i[\boldsymbol{x}(t_{\text{en}})] = 0$, $i = 0, \ldots, p-1$ yield the following necessary conditions:

$$\boldsymbol{\Lambda}\left(t_{\text{en}}^+\right) = \boldsymbol{\Lambda}\left(t_{\text{en}}^-\right) - \sum_{i=0}^{p-1} \varepsilon_i S^i_{\boldsymbol{x}}[\boldsymbol{x}(t_{\text{en}})] \tag{12}$$

$$H\left(t_{\text{en}}^+\right) = H\left(t_{\text{en}}^-\right) \tag{13}$$

$$\boldsymbol{\Lambda}\left(t_{\text{ex}}^+\right) = \boldsymbol{\Lambda}\left(t_{\text{ex}}^-\right) \tag{14}$$

$$H\left(t_{\text{ex}}^+\right) = H\left(t_{\text{ex}}^-\right) \tag{15}$$

Equation (12) admits the discontinuities in the costate variables at the entry point t_{en}. Because the state inequality constraint does not depend on time explicitly, the Hamiltonian is continuous at t_{en} for the ALS problem. The continuity of the controls, $u(t)$, is assumed at t_{en}:

$$\boldsymbol{u}\left(t_{\text{en}}^-\right) = \boldsymbol{u}\left(t_{\text{en}}^+\right) = \boldsymbol{u}_b(t_{\text{en}}) \tag{16}$$

We determine the boundary control $\boldsymbol{u}_b$ by using $S^p(\boldsymbol{x}, \boldsymbol{u}) = 0$ over the boundary arcs.[14] Similarly, we have the assumption of the continuity of $\boldsymbol{u}(t)$ at t_{ex}:

$$\boldsymbol{u}\left(t_{ex}^-\right) = \boldsymbol{u}\left(t_{ex}^+\right) = \boldsymbol{u}_b(t_{ex}) \tag{17}$$

For the ALS problem, S^p is dependent on only one free control variable, the angle of attack. Thus, Eq. (10) yields the multiplier $\eta(t)$ explicitly on the boundary arcs for a scalar boundary control, along the optimal trajectory, as S_u^p is not zero:

$$\eta(t) = -\frac{G_u + \Lambda^T f_u}{S_u^p} \tag{18}$$

The t_{ex} can be obtained by using Eq. (17). We use the control $u(t)$ from the condition $G_u + \Lambda^T f_u = 0$ on the interior arcs. Then, for the problem with inequality constraints, Eqs. (6a) and (11) are the equations of state and costate variables.

Model of the Aerospace Vehicle

The physical model chosen for this study is the ALS as described in Ref. 1. This ALS configuration (Fig. 1) consists of a core and a booster module assembled in parallel to deliver large payloads into a low Earth orbit. The core contains three engines, and the booster contains seven engines. The ALS is designed as an uncrewed expendable launch vehicle system, which can launch payloads more frequently while reducing the cost per pound of payload into space. At burnout of the booster, separation occurs and the core continues the flight. Before staging time, the combination of the booster and the core is referred to as the first stage, and the second stage refers to only the core vehicle after the jettison of the booster. The payload is to be inserted into a 80×150 nm Earth orbit at perigee after being launched vertically by the ALS. From Ref. 1, the three-degree-of-freedom equations of motion relative to the Earth are

$$\dot{\lambda} = \frac{V \cos\gamma \cos\psi}{r \cos\tau} \tag{19a}$$

$$\dot{\tau} = \frac{V \cos\gamma \sin\psi}{r} \tag{19b}$$

$$\dot{h} = V \sin\gamma \tag{19c}$$

$$\dot{V} = \frac{1}{m}[T\cos(\alpha+\delta) - D - mg\sin\gamma] + r\omega^2 \cos\tau[\cos\tau\sin\gamma - \sin\tau\cos\gamma\sin\psi] \tag{19d}$$

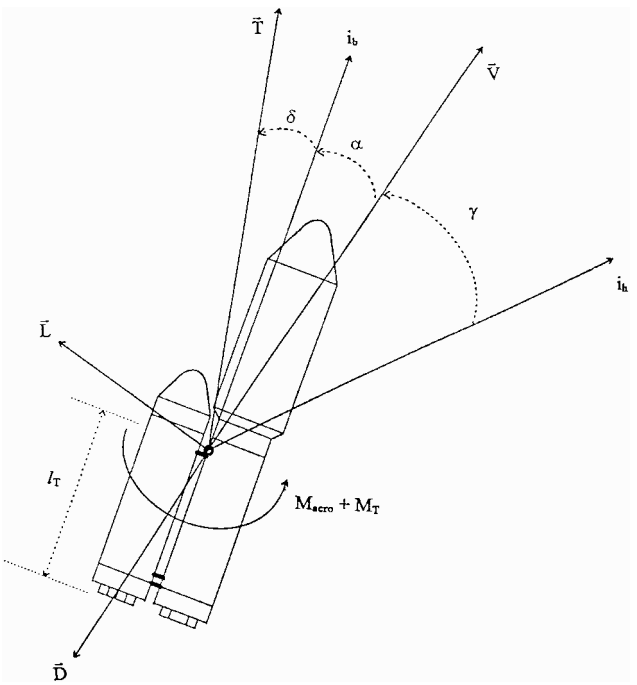

Fig. 1 ALS.

$$\dot{\gamma} = \frac{1}{mV}\{[T\sin(\alpha+\delta) + L]\cos\mu - mg\cos\gamma\} + \frac{V\cos\gamma}{r} + 2\omega\cos\tau\cos\psi + \frac{r\omega^2}{V}\cos\tau[\cos\tau\cos\gamma + \sin\tau\sin\gamma\sin\psi] \tag{19e}$$

$$\dot{\psi} = -\frac{1}{mV\cos\gamma}[T\sin(\alpha+\delta) + L]\sin\mu - \frac{V}{r}\tan\tau\cos\gamma\cos\psi + 2\omega[\cos\tau\tan\gamma\sin\psi - \sin\tau] - \frac{r\omega^2}{V\cos\gamma}\cos\tau\sin\tau\cos\psi \tag{19f}$$

$$\dot{m} = -\frac{c}{I_{sp}g_s}T_{vac} \tag{19g}$$

The physical model for the ALS is described in detail in Ref. 1. The thrust model is given by

$$T = c[T_{vac} - pA_e] \tag{20}$$

Density and pressure are modeled as the following exponential functions of altitude:

$$\rho = \rho_s e^{-h/h_1} \tag{21}$$

$$p = p_s e^{-h/h_2} \tag{22}$$

The Earth is assumed to be a rotating, spherical body with an inverse square gravity field

$$g = g_s(r_s/r)^2 \tag{23}$$

The speed of sound is given using the perfect gas law

$$a = \sqrt{\beta(p/\rho)} \tag{24}$$

The dynamic pressure, the drag, and the lift are defined as

$$q = \tfrac{1}{2}\rho V^2 \tag{25}$$

$$D = qA_bC_D \tag{26}$$

$$L = qA_bC_L \tag{27}$$

and C_D, C_L, and C_m are modeled as polynomials in α during the first stage:

$$C_D = C_{D0}(M) + C_{D1}(M)\alpha + C_{D2}(M)\alpha^2 + C_{D3}(M)\alpha^3 \tag{28a}$$

$$C_L = C_{L1}(M)\alpha \tag{28b}$$

$$C_m = C_{m0}(M) + C_{m1}(M)\alpha \tag{28c}$$

After staging, the vehicle flies at hypersonic velocities, the aerodynamic force coefficients are independent of the Mach number, and pitching moments are assumed to be negligible. The aerodynamic models for the second stage are

$$C_D = C_{D0} + C_{D2}\alpha^2 \tag{29a}$$

$$C_L = C_{L1}\alpha + C_{L2}\alpha|\alpha| \tag{29b}$$

The drag coefficient, the lift coefficient, and the pitching moment coefficient are given in tabular form as functions of Mach number and α in Refs. 1 and 2. The aerodynamic coefficients are interpolated by the least-squares method and the cubic spline method. When the sign of α is changed, the sign of C_{L2} is also changed for the second stage. Note that, during the second stage, the drag coefficient is a symmetric function of α, whereas the lift coefficient is an antisymmetric function of α.

Problem Statement

We augment the ALS system with the additional parameter equations to find exact switching structure and final time.

For the first stage:

$$\dot{t}_{\text{en}} = 0, \qquad \dot{t}_{\text{ex}} = 0 \tag{30a}$$

For the second stage:

$$\dot{t}_f = 0 \tag{30b}$$

Equation (30b) is an additional state equation that handles the free final time as a parameter. This parameter is guessed and is also adjusted by the Newton method. This additional parameter requires an additional costate. Thus, two additional differential equations are introduced when the free final time is treated as a parameter.

Performance Index

For the problem at hand, it is required to find the optimal trajectory that maximizes the final mass of the ALS. Transferring the maximization problem into a minimization problem yields

$$J = -m_f/m_{\text{ref}} \tag{31}$$

The magnitude -1.0 of the performance index indicates that the reference mass is inserted into orbit without extra fuel.

Initial Conditions

The ALS is launched vertically from the Earth with the following initial conditions[1] at $t = 0$ s:

$$\lambda(0) = -80.54\,\text{deg}, \qquad \tau(0) = 28.5\,\text{deg}$$
$$h(0) = 0\,\text{ft}, \qquad V(0) = 0\,\text{ft/s} \tag{32a}$$

$$\gamma(0) = 90.0\,\text{deg}, \qquad \psi(0) = 0\,\text{deg}$$
$$m(0) = 108{,}574.93\,\text{slug} \tag{32b}$$

The heading angle is not defined during the 3 s of vertical flight. When $V = 0$, the equations for $\dot{\gamma}$ and $\dot{\psi}$ have singularities, whereas $\gamma = 90$ deg causes the same effect in the $\dot{\psi}$ equation. To remove the singularity due to the velocity, the ALS is vertically flown for 3 s with the angle of attack and the velocity roll angle chosen such that $\dot{\gamma}$ and $\mu = 0$. To avoid the singularity due to $\gamma = 90$ deg, the vehicle is then pitched over by flying it for 1 s at a constant pitch rate. The velocity roll angle is chosen such that $\dot{\psi}$ is zero.[1] The angle of attack is given by the following equation during the fourth second[15]:

$$\alpha(t) = \pi/2 - \gamma - 0.02(t - 3) \tag{33}$$

The optimization uses the state at this time as the initial condition. Explicitly, the initial conditions at time $t = 4$ s are given by[15]

$$\lambda(4) = -80.558\,\text{deg}, \qquad \tau(4) = 28.5\,\text{deg}$$
$$h(4) = 109.69\,\text{ft}, \qquad V(4) = 55.34\,\text{ft/s} \tag{34a}$$

$$\gamma(4) = 89.526\,\text{deg}, \qquad \psi(4) = 0\,\text{deg}$$
$$m(4) = 106{,}897.68\,\text{slug} \tag{34b}$$

Final Conditions

Final boundary conditions are specified to satisfy orbit size, shape, inclination, vehicle position, and orbit injection. The vehicle must be inserted into the specified orbit at the perigee. The desired injection point is 80×150 nm transfer orbit of 28.5-deg inclination i. The desired value of h_p is 80 nm, and the desired value of h_a is 150 nm. To achieve the desired orbit, four final conditions should be satisfied. These are the altitude, the inertial velocity, the flight-path angle, and the orbital inclination. The perigee altitude of the orbit, h_p, must equal to the final altitude h_f. The inertial velocity at t_f must be constrained to satisfy the following relationship[1]:

$$V_{if} = \sqrt{\frac{g_s r_s^2 (e+1)}{r_p}} \tag{35}$$

For the vehicle to be inserted into orbit at the perigee, the final flight-path angle should be zero. As a consequence, the terminal equality constraints are the following:

$$h_{f_s} = 486{,}080\,\text{ft}, \qquad V_{f_s} = 25{,}776.9\,\text{ft/s}$$
$$\gamma_{f_s} = 0\,\text{deg}, \qquad i_{f_s} = 28.5\,\text{deg} \tag{36}$$

The inertial velocity and inclination are calculated by[1]

$$V_i = (V^2 + 2Vr\omega\cos\gamma\cos\psi\cos\tau + r^2\omega^2\cos^2\tau)^{\frac{1}{2}} \tag{37}$$

$$\cos i = \frac{\cos\tau(V\cos\gamma\cos\psi + r\omega\cos\tau)}{(V^2\cos^2\gamma + 2Vr\omega\cos\gamma\cos\psi\cos\tau + r^2\omega^2\cos^2\tau)^{\frac{1}{2}}} \tag{38}$$

In summary, the final point constraints are

$$h_f = h_{f_s} \tag{39a}$$

$$V_f = V_{f_s} \tag{39b}$$

$$\gamma_f = \gamma_{f_s} \tag{39c}$$

$$\cos(i_f) = \cos\left(i_{f_s}\right) \tag{39d}$$

For the ALS problem, there are seven known initial state variables at t_0 and two fixed state variables [Eqs. (39a) and (39c)] at t_f. Equation (3) contains two boundary equations [Eqs. (39b) and (39d)] at final time t_f:

$$\Theta_1 \equiv V_{f_s} - (V^2 + 2Vr\omega\cos\gamma\cos\psi\cos\tau + r^2\omega^2\cos^2\tau)^{\frac{1}{2}} = 0 \tag{40}$$

$$\Theta_2 \equiv \frac{\cos\left(i_{f_s}\right) - \cos\tau(V\cos\gamma\cos\psi + r\omega\cos\tau)}{(V^2\cos^2\gamma + 2Vr\omega\cos\gamma\cos\psi\cos\tau + r^2\omega^2\cos^2\tau)^{\frac{1}{2}}} = 0 \tag{41}$$

From transversality conditions, we obtain

$$\Lambda_\lambda(t_f) = 0 \tag{42a}$$

$$\Lambda_{t_f}(t_f) = 0 \tag{42b}$$

$$\Lambda_m(t_f) = -\frac{1}{m_{\text{ref}}} \tag{42c}$$

$$\Lambda_\tau(t_f) - \nu_1\left.\frac{\partial\Theta_1}{\partial\tau}\right|_{t_f} - \nu_2\left.\frac{\partial\Theta_2}{\partial\tau}\right|_{t_f} = 0 \tag{42d}$$

$$\Lambda_V(t_f) - \nu_1\left.\frac{\partial\Theta_1}{\partial V}\right|_{t_f} - \nu_2\left.\frac{\partial\Theta_2}{\partial V}\right|_{t_f} = 0 \tag{42e}$$

$$\Lambda_\psi(t_f) - \nu_1\left.\frac{\partial\Theta_1}{\partial\psi}\right|_{t_f} - \nu_2\left.\frac{\partial\Theta_2}{\partial\psi}\right|_{t_f} = 0 \tag{42f}$$

From Eqs. (42d) and (42e), we can calculate ν_1 and ν_2 as follows:

$$\nu_2 = \left[\Lambda_V(t_f) - \Lambda_\tau(t_f)\left.\frac{\partial\Theta_1}{\partial V}\right|_{t_f} \Big/ \left.\frac{\partial\Theta_1}{\partial\tau}\right|_{t_f}\right] \Big/ \left[\left.\frac{\partial\Theta_2}{\partial V}\right|_{t_f} - \left.\frac{\partial\Theta_2}{\partial\tau}\right|_{t_f}\left.\frac{\partial\Theta_1}{\partial V}\right|_{t_f} \Big/ \left.\frac{\partial\Theta_1}{\partial\tau}\right|_{t_f}\right] \tag{43a}$$

$$\nu_1 = \left[\Lambda_\tau(t_f) - \nu_2\left.\frac{\partial\Theta_2}{\partial\tau}\right|_{t_f}\right] \Big/ \left.\frac{\partial\Theta_1}{\partial\tau}\right|_{t_f} \tag{43b}$$

With Eqs. (43a) and (43b), Eq. (42f) becomes another boundary equation at the final time. Thus, we only have three boundary

equations at the final time: Eqs. (40), (41), and (42f). There are 16 differential equations including the additional state and costate equations for the free final time parameter. There are 16 unknowns (8 unknowns at t_0 and 8 unknowns at t_f) and 16 known boundary conditions; there are seven given initial states $x(t_0)$, $\Lambda_{t_f}(t_0) = 0$, Eqs. (39a), (39c), (40), (41), (42a), (42b), (42c), and (42f). Thus, the two-point boundary problem can be completely solved with these boundary conditions.

Controls

The aerodynamic yawing moment is assumed to be controlled to zero, whereas the angle of attack and the velocity roll angle are treated as control variables. Thus, the sideslip angle is zero throughout the trajectory. The pitching moment due to the thrust and aerodynamics is controlled to be zero. This trimmed flight condition is effected by the gimbal angle, which is created by orienting the thrust with respect to the ALS body axis so that the pitching moment is zero. Therefore, the trimmed flight is controlled by finding a gimbal angle, that forces the pitching moment to be zero at any instant of time. Explicitly, this yields the following control constraint:

$$M_{\text{aero}}(\alpha) + M_T = 0 \tag{44}$$

Equation (44) can be written as

$$q S_b l C_{m\text{cg}} - T l_T \sin\delta = 0 \tag{45}$$

To calculate the gimbal angle δ from Eq. (45), we need the value of the location of the vehicle center of gravity. Numerical studies show that the dynamic pressure goes to zero in the second stage; hence, the gimbal angle is zero from Eq. (45). Thus, trimmed flight is assumed during only the first stage. A reference to untrimmed flight indicates the situation where the moment equation is neglected.

Equation (6e) is solved for the free controls. The first derivative of the Hamiltonian with respect to the velocity roll angle μ is

$$H_\mu = \Lambda_\gamma \dot{\gamma}_\mu + \Lambda_\psi \dot{\psi}_\mu = 0 \tag{46}$$

Equation (46) can be solved for $\tan\mu$. Then the velocity roll angle is calculated using the following equation:

$$\tan\mu = -\frac{\Lambda_\psi}{\Lambda_\gamma \cos\gamma} \tag{47}$$

The first derivative of the Hamiltonian with respect to the angle of attack α is

$$H_\alpha = \Lambda_V \dot{V}_\alpha + \Lambda_\gamma \dot{\gamma}_\alpha + \Lambda_\psi \dot{\psi}_\alpha = 0 \tag{48}$$

Then, the angle of attack is calculated using the following equation:

$$\begin{aligned} 0 = {} & \frac{\Lambda_V}{m}\left[-T\sin(\alpha+\delta)\left(1+\frac{\partial\delta}{\partial\alpha}\right) - \frac{\partial D}{\partial\alpha}\right] \\ & + \frac{\Lambda_\gamma}{mV}\left\{\left[T\cos(\alpha+\delta)\left(1+\frac{\partial\delta}{\partial\alpha}\right) + \frac{\partial L}{\partial\alpha}\right]\cos\mu\right\} \\ & + \frac{\Lambda_\psi}{mV\cos\gamma}\left\{-\left[T\cos(\alpha+\delta)\left(1+\frac{\partial\delta}{\partial\alpha}\right) + \frac{\partial L}{\partial\alpha}\right]\sin\mu\right\} \end{aligned} \tag{49}$$

The angle of attack and gimbal angle satisfying the Eqs. (45) and (49) simultaneously can be obtained using the Newton–Raphson method.

A second-order necessary condition, the Legendre condition, states that the second derivative of the Hamiltonian with respect to the controls must be greater than or equal to zero for the performance index to be at a minimum. Thus, $H_{\alpha\alpha}$, $H_{\mu\mu}$, and $H_{\alpha\alpha}H_{\mu\mu} - H_{\alpha\mu}^2$ must be greater than or equal to zero for the performance index to be at a minimum. These conditions are enforced through numerical checks.

Internal Boundary Conditions and Inequality Constraints

The discontinuity in the variation of mass occurs when the booster is separated at the staging time. The staging time $t_s = 153.54$ s is known because the booster is separated when all of the propellant in the booster has been burned out. The problem can be divided into two sections with respect to the staging time, the first stage and the second stage. Because we know the staging time, we can consider the problem as a fixed final time problem in the first stage and a free final time problem in the second stage, whereas the whole problem is a free final time problem. The known final time for the first stage is the staging time t_s. The conditions at the staging time are (except mass)

$$\boldsymbol{x}(t_s^-) = \boldsymbol{x}(t_s^+) \tag{50a}$$

$$m(t_s^-) = m(t_s^+) + 6740.85\,\text{slug} \tag{50b}$$

$$\Lambda(t_s^-) = \Lambda(t_s^+) \tag{50c}$$

There are no explicit constraints on the states at the staging time, and the staging point is not significant.

A dynamic pressure constraint is imposed as a state variable inequality constraint by limiting it to $q_{\max} = 650\,\text{lb/ft}^2$. That is,

$$S(\boldsymbol{x}) \equiv q(\boldsymbol{x}) = \tfrac{1}{2}\rho V^2 \le 650\,\text{lb/ft}^2 \tag{51}$$

This constraint, being first order in nature, leads to jumps in the altitude and velocity costates. We determine the angle of attack α_b as the boundary control over the boundary arc using the following equation:

$$\begin{aligned} \dot{S}(\boldsymbol{x},\boldsymbol{u}) = {} & -[1/(2h_1)]\rho V^3 \sin\gamma \\ & + \rho V[(1/m)\{T\cos(\alpha+\delta) - D - mg\sin\gamma\} \\ & + r\omega^2\cos\tau\{\cos\tau\sin\gamma - \sin\tau\cos\gamma\sin\psi\}] = 0 \end{aligned} \tag{52}$$

The additional internal boundary conditions at the junction points are from Eq. (12) to Eq. (17), and $q(t_{\text{en}}) = 650\,\text{lb/ft}^2$. The internal boundary conditions at each subinterval except for the junction points are satisfied by the continuity of state and costate variables in the multiple shooting method.

Multiple Shooting Method

Many numerical algorithms to solve optimal control problems have been developed. Indirect methods are theoretically based on the minimum principle, which characterizes the set of optimal states and controls in terms of the solution of a boundary-value problem. One of the indirect methods is the shooting method, which yields solutions of high precision. The shooting method is a second-order method and, hence, is very sensitive to small changes of costate initial conditions. Shooting methods have the associated difficulties caused by instability of the initial value problem for the system of differential equations and by the requirement for good initial guesses for the iterative solutions of nonlinear problems. To overcome the difficulties in the direct shooting methods, multiple shooting methods can be used for solving the problems. The multiple shooting technique divides the interval from t_0 to t_f into several subintervals. The result is that the dimension of the problem is increased, but the sensitivity of the solutions to the boundary-value variables is reduced. The application of multiple shooting methods to the solution of boundary-value problems can be found in Refs. 16–18. The multiple shooting technique is simply a multipoint version of the direct shooting method. Using this method, the solution of an optimal control problem still amounts to solving a set of algebraic equations at each subinterval. These multiple shooting methods require the continuity of state and costate variables at the boundary of each subinterval where jump conditions are not specified. The multiple shooting methods use the same technique as the nominal shooting methods to calculate corrections to the values of states and costates at the boundary of these small subintervals.

Because the basic idea of multiple shooting is to subdivide the interval $[t_0, t_f]$, one may integrate in one direction (usually forward direction) up to certain nodes (method I) and one may integrate in

both directions up to certain matching nodes (method II).[18] In cases where the integration costs are independent of the direction of integration, the total integration costs are about the same because the greater part of computing time is spent in the numerical integration of the subtrajectories. When both methods have an equivalent set of nodes, method II treats about half the number of unknown variables, and the size of the Jacobian matrix of method II is half of the Jacobian matrix size of method I. Therefore, the numerical code is developed by method II in this paper to solve the ALS problem. Generally, method II includes method I as a special case. The different subtrajectories are computed in a mutually independent way. This structure of multiple shooting is readily adapted to parallel techniques to get a considerable speed-up of the computation. At entry point t_{en} and exit point t_{ex}, the Jacobian submatrices and corresponding error vectors for the ALS problem must be modified to include the constraints: $u(t_{en}^-) = u(t_{en}^+)$, $S(t_{en}) = S_{limit}$, and $u(t_{ex}^-) = u(t_{ex}^+)$. With this multiple shooting structure, the internal and terminal boundary conditions can be exactly satisfied. The time interval during the first stage is divided into 12 subintervals, and during the second stage it is divided into 4 subintervals.

Hodograph Analysis

The hodograph at a given time and state is the set of all possible state rates that can be attained by varying the controls within its allowed domain. For any fixed state vector, the set of admissible state rates is obtained by letting the controls vary within their allowed domains. Thus, an m-dimensional manifold is generated in the n-dimensional state rate space (in our case $n = 7$ and $m = 2$). For the problem under consideration, it suffices to look only at the $\dot{V}$, $\dot{\gamma}$, and $\dot{\psi}$ components of the state rate vectors. The right-hand sides of all other state rates are independent of the controls and, hence, only trace a single point as the controls are varied. Therefore, the problem is reduced to visualizing the projection of the hodograph into the $\dot{V}$, $\dot{\gamma}$, and $\dot{\psi}$ space.

As we are mainly interested in convexity issues, we do not lose any information by visualizing the hodograph in a coordinate system (k_1–k_2–k_3), which is scaled and shifted with respect to the $\dot{V}$, $\dot{\gamma}$, and $\dot{\psi}$ system. The (k_1–k_2–k_3) axes are defined as follows:

$$k_1 = m\dot{V} + mg\sin\gamma - mr\omega^2\cos\tau(\cos\tau\sin\gamma - \sin\tau\cos\gamma\sin\psi) \tag{53a}$$

$$k_2 = mV\left[\dot{\gamma} - \frac{V\cos\gamma}{r} - 2\omega\cos\tau\cos\psi - \frac{r}{V}\omega^2\cos\tau(\cos\tau\cos\gamma + \sin\tau\sin\gamma\sin\psi)\right] + mg\cos\gamma \tag{53b}$$

$$k_3 = -mV\cos\gamma\left[\dot{\psi} + \frac{V}{r}\tan\tau\cos\gamma\cos\psi - 2\omega(\cos\tau\tan\gamma\sin\psi - \sin\tau) + \frac{r\omega^2\cos\tau\sin\tau\cos\psi}{V\cos\gamma}\right] \tag{53c}$$

It can also be verified from equations of motion that

$$k_1 \equiv T\cos(\alpha+\delta) - D \tag{54a}$$

$$k_2 \equiv [T\sin(\alpha+\delta) + L]\cos\mu \tag{54b}$$

$$k_3 \equiv [T\sin(\alpha+\delta) + L]\sin\mu \tag{54c}$$

From Eqs. (54), obviously, the hodograph in the (k_1–k_2–k_3) system can be obtained by rotating the hodograph in the (k_1–k_2) system about the k_1 axis. The hodograph in the (k_1–k_2) system can be visualized using the following method. Let σ be an auxiliary parameter that varies from -1 to $+1$, boundaries excluded. Then, $\alpha^*(\sigma)$ and $\delta^*(\sigma)$ are calculated by using the following equation:

$$[\alpha^*(\sigma), \delta^*(\sigma)] = \underset{\alpha\in\Omega}{\arg\max}\, Q(\sigma) \tag{55}$$

where

$$\Omega = \{\alpha \in R, \delta \in R \mid \text{pitching moment} = 0 \text{ [Eq. (45)]}\} \tag{56}$$

and

$$Q(\sigma) = \sqrt{1-\sigma^2}[T\cos(\alpha+\delta) - D] + \sigma[T\sin(\alpha+\delta) + L] \tag{57}$$

This procedure equivalently yields the controls $[\alpha^*(\sigma), \delta^*(\sigma)]$ that minimize the Hamiltonian

$$H = \Lambda_{k_1}k_1 + \Lambda_{k_2}k_2 + \Lambda_{k_3}k_3 + \text{terms independent of controls} \tag{58}$$

for the case where $\Lambda_{k_1} = -\sqrt{(1-\sigma^2)}$, $\Lambda_{k_2} = -\sigma$, and $\Lambda_{k_3} = 0$. Note that as σ is varied, Λ_{k_1} already defined remains negative, which is required for the existence of a bounded control. The hodograph in the k_1–k_2 system is obtained by plotting the curve

$$k_1(\sigma) = T\cos[\alpha^*(\sigma) + \delta^*(\sigma)] - D|_{\alpha^*(\sigma)} \tag{59a}$$

$$k_2(\sigma) = T\sin[\alpha^*(\sigma) + \delta^*(\sigma)] + L|_{\alpha^*(\sigma)} \tag{59b}$$

Rotation of the hodograph in the described (k_1–k_2) system about the k_1 axis results in the hodograph in the (k_1–k_2–k_3) system. It should be noted that a necessary condition for convexity of the hodograph in the (k_1–k_2–k_3) system is that in the (k_1–k_2) system, the maximum k_1 value is obtained at $k_2 = 0$.

Results and Discussion

Ascent optimal trajectories of the ALS have been computed to maximize the final mass of the vehicle. Because the problem is very sensitive to initial guesses, the multiple shooting method with 16 subintervals is used to reduce the sensitivity. The Hamiltonian will be a constant during the first stage because the final time is fixed and the Hamiltonian does not depend explicitly on time, whereas the Hamiltonian is zero in the second stage because the final time is free and the Hamiltonian does not depend explicitly on time. A jump discontinuity in the Hamiltonian is evident at the staging time.

Optimal trajectories have been computed for the two aerodynamic models with and without the dynamic pressure constraint. Figures 2–7, respectively, show the time histories of the longitude, the latitude, the altitude, the velocity, the flight-path angle, and the heading angle. A and B in Figs. 2–14 denote the aerodynamic data in Refs. 1 and 2, respectively. The variations of the latitude and the heading angle are very small in this particular example, while the longitude increases by approximately 10 deg. Therefore, it is possible to approximate the three-dimensional equations of motion to obtain simple planar equations of motion. At the staging time, the velocity history has a discontinuity due to the mass and thrust discontinuities caused by separation of the booster. It is evident that the aerodynamic model effects on the longitude, the altitude, the velocity, and the mass are insignificant and on the latitude, the flight-path

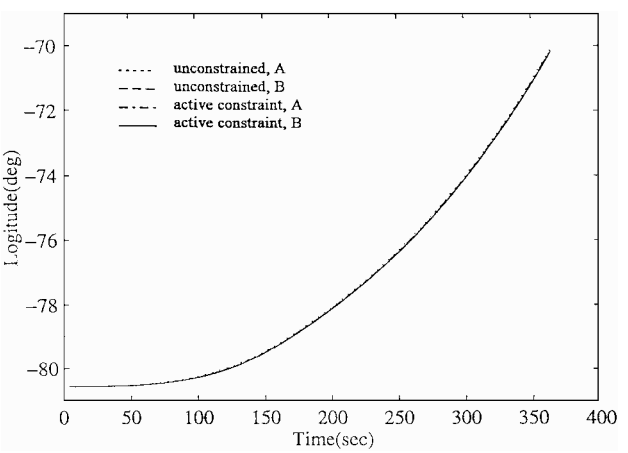

Fig. 2 Time histories of the longitude.

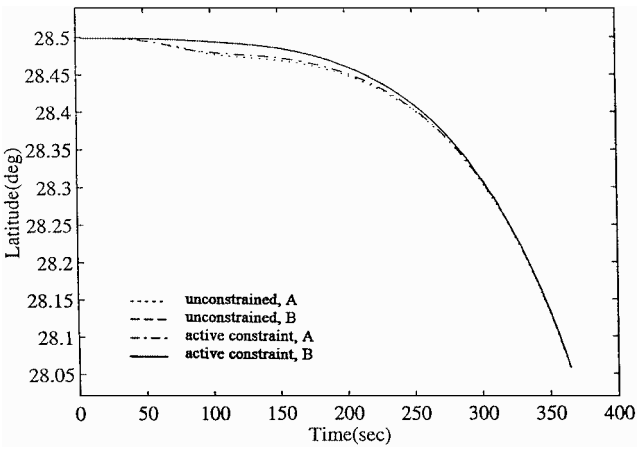

Fig. 3 Time histories of the latitude.

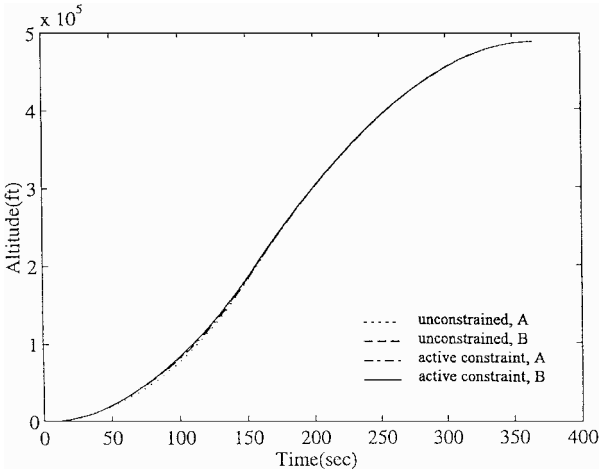

Fig. 4 Time histories of the altitude.

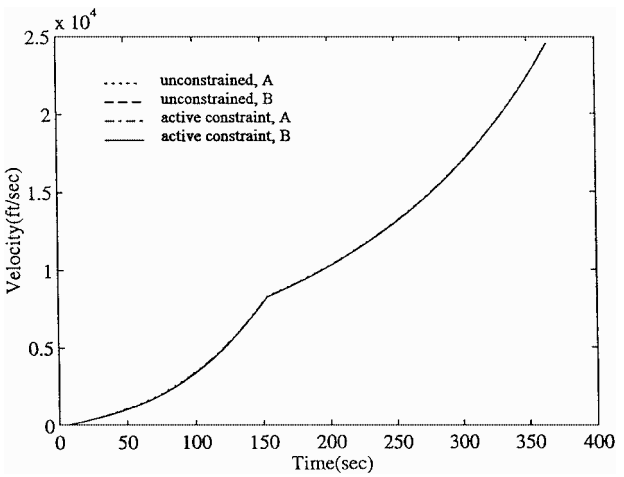

Fig. 5 Time histories of the velocity.

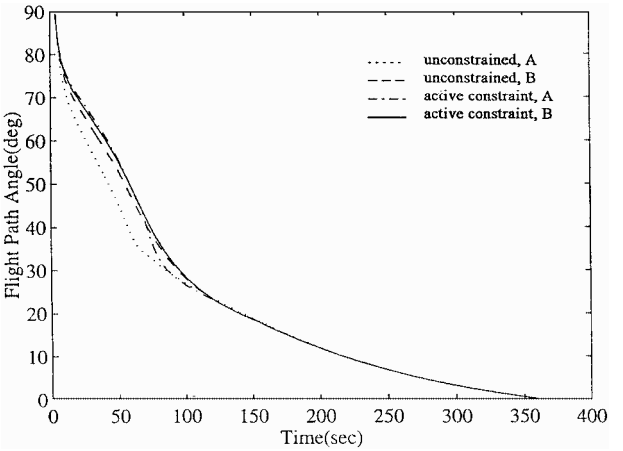

Fig. 6 Time histories of the flight-path angle.

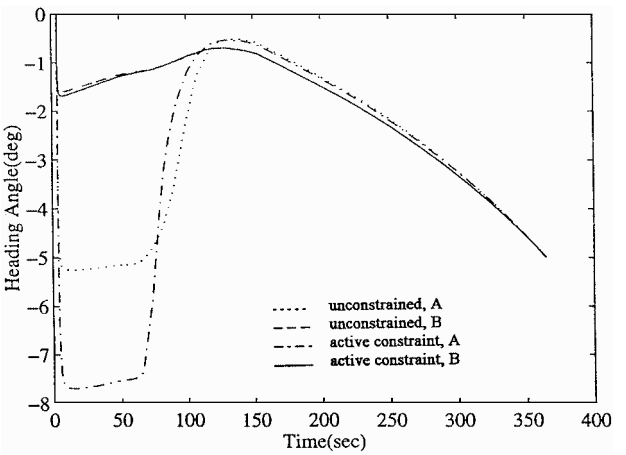

Fig. 7 Time histories of the heading angle.

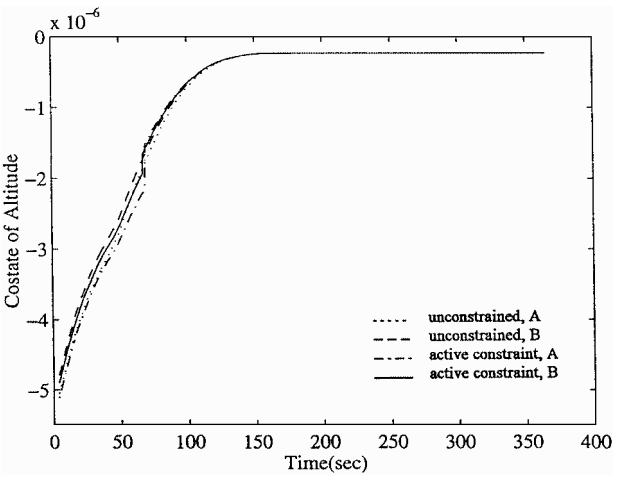

Fig. 8 Costate of the altitude vs time.

angle, and the heading angle are only slight. Figures 8–10 show the time histories of the costate variables of the altitude, the velocity, and the flight-path angle, respectively. As expected, the jumps in costates of the altitude and the velocity occur due to the internal boundary conditions caused by the inequality constraint. The costate of the flight-path angle strongly affects the velocity roll angle history, especially when its magnitude is very small compared with that of the costate of the heading angle.

Figures 11–14 show the time histories of the velocity roll angle, the angle of attack, the gimbal angle, and the dynamic pressure, respectively. The velocity roll angle history shows sharp variations, especially when the constraint is active. A small gimbal angle deflection is needed to satisfy trimmed flight conditions. Because only the core vehicle remains during the second stage, the pitching moments are assumed to be zero such that the gimbal angle is zero in the second stage. The dynamic pressure constraint is active for a small interval of time. Compared with the unconstrained cases, the angle of attack decreases during passage through the maximum constrained dynamic pressure. Because the drag coefficient is a symmetric function of α while the lift coefficient is an antisymmetric function of α for the second stage, it is clear that the equations of motion remain unchanged during the second stage ($\delta = 0$) if the sign of α is reversed (solid line and dash-dot line in Fig. 12) and a 180-deg phase shift (solid line and dash-dot line in Fig. 11) is introduced in μ; i.e., the signs of $\sin\mu$ and $\cos\mu$ are also reversed. This situation gives rise to two different types of optimal controls,

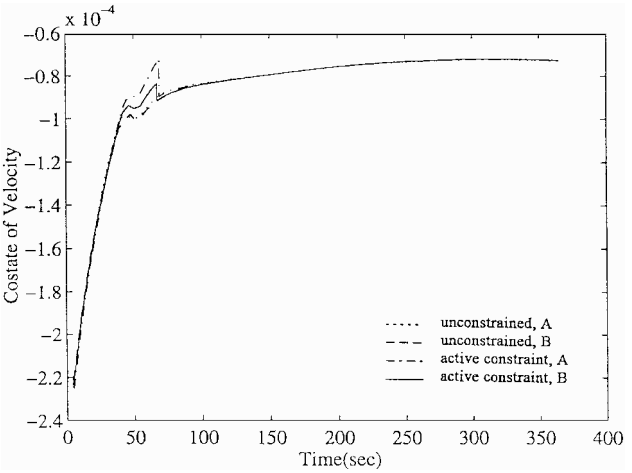

Fig. 9 Costate of the velocity vs time.

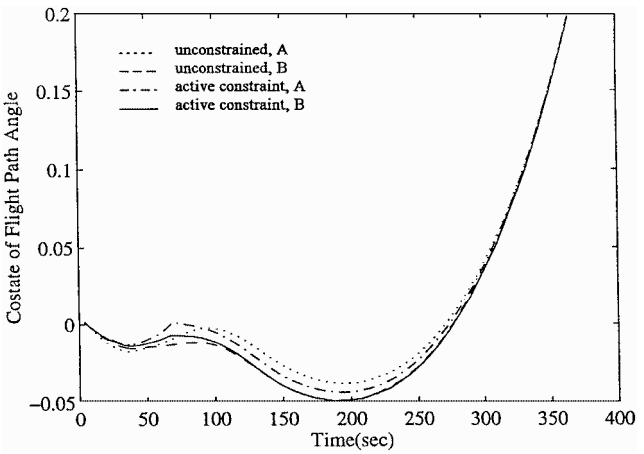

Fig. 10 Costate of the flight-path angle vs time.

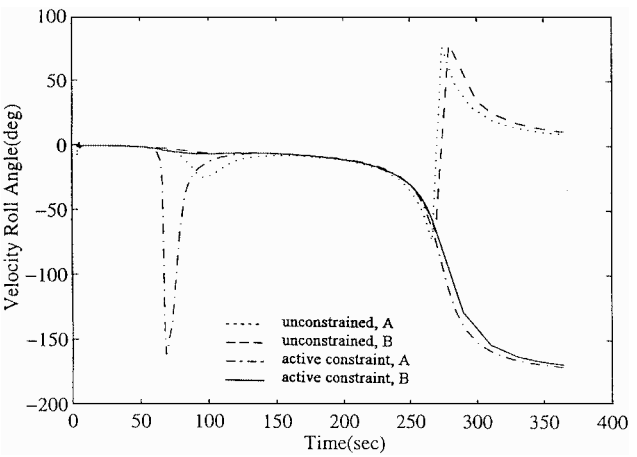

Fig. 11 Time histories of the velocity roll angle.

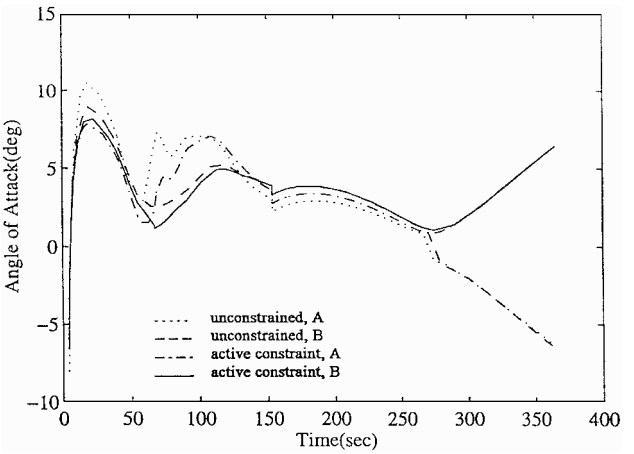

Fig. 12 Time histories of the angle of attack.

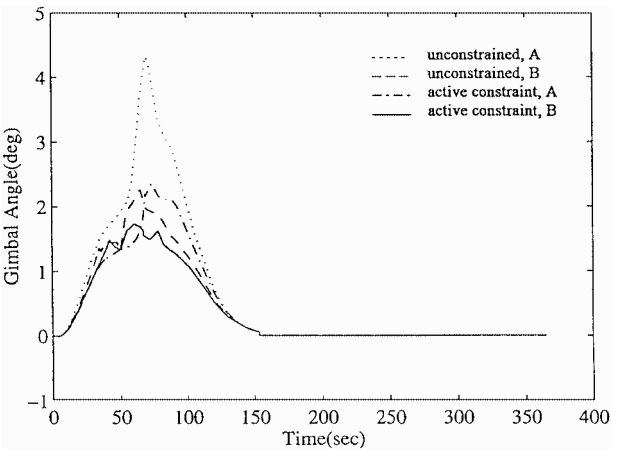

Fig. 13 Time histories of the gimbal angle.

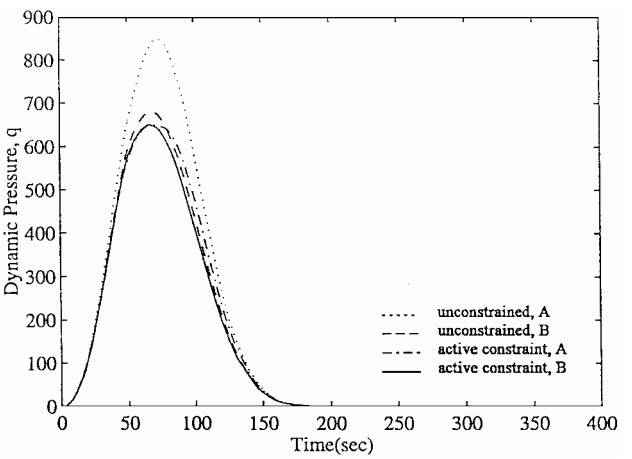

Fig. 14 Time histories of the dynamic pressure.

as shown in Ref. 5, and the two types of solutions can be pieced together at various points of time. However, it is preferable to use the optimal velocity roll angle profile that requires a smooth roll angle profile rather than a sequence of roll reversals. This means that, during the second stage, two different types of control histories are possible due to nonuniquenessof the controls. These control histories are shown in Figs. 11 and 12.

For the unconstrained cases, the aerodynamic data in Ref. 1 yielded a performance index of -1.031659 and the final time of 364.14 s, whereas those in Ref. 2 yielded a performance index of -1.020098 and a final time of 364.63 s. When the 650-lb/ft^2 dynamic pressure constraint is imposed, the aerodynamic model in Ref. 1 yielded a performance index of -1.027255 and the final time of 364.32 s, whereas those in Ref. 2 yielded a performance index of -1.019723 and a final time of 364.64 s. In terms of physical parameters, a performance index of -1.019723 means that 104.9 slug of fuel remains when the ALS is inserted into a desired orbit whereas a performance index of -1.027255 means 105.7 slug of remnant fuel. This fuel weight could be converted into extra payload. The internal boundary conditions and the dynamic pressure constraint are exactly satisfied. For the constrained case with the aerodynamic model in Ref. 2, the trajectory enters the boundary arc at $t_{en} = 66.9680$ s and exits from the arc at $t_{ex} = 66.9938$ s. The length of the boundary arc is small, 0.0258 s. From Fig. 15 with the aerodynamic model in Ref. 2, we know that the final mass of the ALS is reduced as the maximum dynamic pressure value is

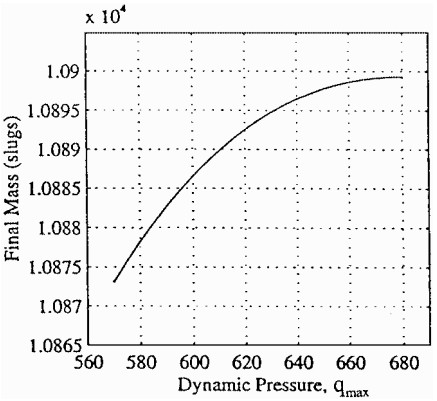

Fig. 15 Constrained dynamic pressure value vs the final mass.

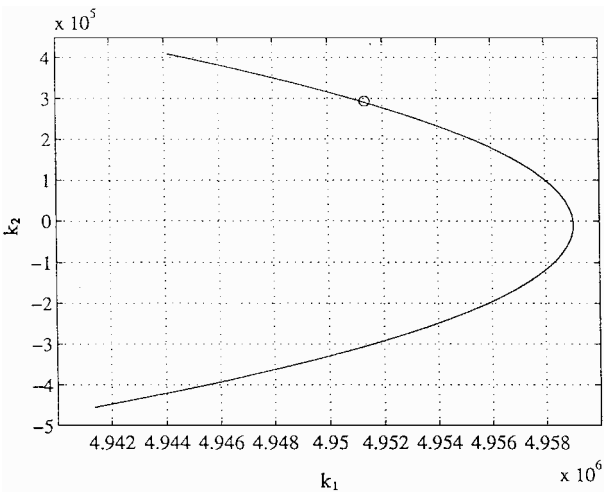

Fig. 16 Hodograph during the first stage.

lowered. The final mass is about 10,878 slug for $q_{\max} = 580$ lb/ft^2, whereas the final mass is about 10,899 slug for unconstrained case (about $q_{\max} = 680$ lb/ft^2). Thus, only about 0.2% less mass compared to that by the unconstrained trajectory is placed in orbit by the constrained optimal trajectory ($q_{\max} = 580$ lb/ft^2).

Using the aerodynamic data in Ref. 2, Fig. 16 shows the hodographs at a selected point of time in the first stage. It is observed that the hodograph in the $(k_1$–$k_2)$ plane is asymmetric about the k_1 axis in Fig. 16. Furthermore the maximum value of k_1 occurs when k_2 is nonzero. Hence, a nonconvex hodograph is generated when Fig. 16 is rotated about the k_1 axis. During the second stage, the hodograph is convex and symmetric about the k_1 axis. The state rates vary smoothly along the trajectories. The small circle in Fig. 16 shows the respective state rate vectors rotated by $-\mu$ about the k_1 axis. This point is plotted in the hodographs to show that the minimum H process does yield state rates on the convex hull of the hodograph. Note that Eq. (6e) is satisfied by the angle of attack at the instant of time corresponding to Fig. 16. Special mention must be made of the jump discontinuities or chattering controls that can occur for nonconvex hodographs if the small circle is at the maximum k_1 point or the flight-path angle and heading angle costates are both zero during the first stage. This condition is not satisfied here.

Concluding Remarks

This paper presents the maximum final mass trajectories for the ALS, which is designed to deliver large payloads into a low Earth orbit. The trajectories with two different aerodynamic models show that the performance indices obtained are nearly the same, whereas some state and control variables are different. These differences are significant and have profound implications with regard to uncertainty in the aerodynamic data and closed-loop guidance. The dynamic pressure inequality constraint is imposed by limiting it to 650 lb/ft^2. This constraint leads to jumps in costate variables and yields a boundary arc of small duration. The final mass of the ALS is reduced by only a small amount as the maximum dynamic pressure value is lowered. The optimality of the solutions was investigated using hodograph analysis. The hodographs are nonconvex along the optimal trajectories during certain time intervals, but the optimal state rates remain on the convex domain of the respective hodographs and vary smoothly.

Acknowledgments

The author would like to express his sincere appreciation to Srinavas R. Vadali, Department of Aerospace Engineering, Texas A&M University, for providing invaluable encouragement, academic insights and advise, and guidance. The author is also thankful to Hans Seywald of Analytical Mechanics Associates for many illuminating discussions in regard to the hodograph analysis.

References

[1]Shaver, D. A., and Hull, D. G., "Advanced Launch System Trajectory Optimization Using Suboptimal Control," *Proceedings of the AIAA Guidance, Navigation, and Control Conference*, AIAA, Washington, DC, 1990, pp. 892–901 (AIAA Paper 90-3413).

[2]Seywald, M., and Cliff, E. M., "A Feedback Control for the Advanced Launch System," *Proceedings of the AIAA Guidance, Navigation, and Control Conference*, AIAA, Washington, DC, 1991, pp. 172–181 (AIAA Paper 91-2619).

[3]Hodges, D. H., Bless, R. R., Calise, A. J., and Leung, M., "Finite Element Method for Optimal Guidance of an Advanced Launch Vehicle," *Journal of Guidance, Control, and Dynamics*, Vol. 15, No. 3, 1992, pp. 664–671.

[4]Bless, R. R., Hodges, D. H., and Seywald, H., "State-Constraint Booster Trajectory Solutions via Finite Elements and Shooting," *Proceedings of the AIAA Guidance, Navigation, and Control Conference*, AIAA, Washington, DC, 1993, pp. 406–416 (AIAA Paper 93-3747).

[5]Shelton, S. A., "Optimizing the Trajectory of the Advanced Launch System Using the Shooting Method," M.S. Thesis, Dept. of Aerospace Engineering and Engineering Mechanics, Univ. of Texas, Austin, TX, May 1990.

[6]Burkhart, P. D., "Trajectory Optimization Using the Shooting Method for the Advanced Launch System," M.S. Thesis, Dept. of Aerospace Engineering and Engineering Mechanics, Univ. of Texas, Austin, TX, May 1991.

[7]Wirthman, D. J., Park, S.-Y., and Vadali, S. R., "Trajectory Optimization Using the Parallel Shooting Method on a Parallel Computer," *Journal of Guidance, Control, and Dynamics*, Vol. 18, No. 2, 1995, pp. 377–379.

[8]Burkhart, P. D., and Hull, D. G., "Advanced Launch System Trajectory Optimization," *Proceedings of the Spacecraft Mechanics Conference* (Austin, TX), American Astronautical Society, San Diego, CA, 1996, pp. 1185–1196 (AAS Paper 96-168).

[9]Kirk, D. E., *Optimal Control Theory: An Introduction*, 1st ed., Prentice–Hall, Englewood Cliffs, NJ, pp. 227–234.

[10]Bryson, A. E., Denham, W. F., and Dreyfus, S. E., "Optimal Programming Problems with Inequality Constraint, I: Necessary Conditions for Extremal Solutions," *AIAA Journal*, Vol. 1, 1963, pp. 2544–2550.

[11]Jacobson, D. H., Lele, M. M., and Speyer, J. L., "New Necessary Conditions of Optimality for Control Problems with State-Variable Inequality Constraints," *Journal of Mathematical Analysis and Applications*, Vol. 35, No. 2, 1971, pp. 255–284.

[12]McIntyre, J., and Paiewonsky, B., "On Optimal Control with Bounded State Variables," *Advances in Control Systems*, Vol. 5, 1967, pp. 389–419.

[13]Kreindler, E., "Additional Necessary Conditions for Optimal Control with State-Variable Inequality Constraints," *Journal of Optimization Theory and Applications*, Vol. 38, No. 2, 1982, pp. 241–250.

[14]Maurer, H., and Gillessen, W., "Application of Multiple Shooting to the Numerical Solution of Optimal Control Problems with Bounded State Variables," *Computing*, Vol. 15, No. 1, 1975, pp. 105–126.

[15]Wirthman, D. J., "A Parallel Implementation of the Parallel Shooting Method for Trajectory Optimization," M.S. Thesis, Dept. of Aerospace Engineering, Texas A&M Univ., College Station, TX, Dec. 1992.

[16]Roberts, S. M., and Shipman, J. S., "Multipoint Solution of Two-Point Boundary-Value Problems," *Journal of Optimization Theory and Applications*, Vol. 7, No. 4, 1971, pp. 301–318.

[17]Osborne, M. R., "On Shooting Methods for Boundary Value Problems," *Journal of Mathematical Analysis and Applications*, Vol. 27, No. 2, 1969, pp. 417–433.

[18]Deuflhard, P., "Recent Advances in Multiple Shooting Techniques," *Computational Techniques for Ordinary Differential Equations*, edited by I. Glandwell and D. K. Sayers, Academic, New York, 1980, pp. 217–272.

J. D. Gamble
Associate Editor